

## Properties of Nanobelts and Nanotubes Measured by *In Situ* TEM

Zhong Lin Wang\*

School of Materials Science and Engineering, Georgia Institute of Technology, Atlanta, GA 30332-0245, USA

**Abstract:** Characterizing the physical properties of individual nanostructures is challenging because of the difficulty in manipulating the objects of sizes from nanometers to micrometers. Most nanomeasurements have been carried using scanning probe microscopy. In this article, we demonstrate that transmission electron microscopy can be a powerful tool for quantitative measurements of the mechanical and electrical properties of a single nanostructure. Dual-mode resonance of an oxide nanobelt has been observed, and its bending modulus has been measured. An *in situ* technique was demonstrated for measuring the work function at the tip of a carbon nanotube. The ballistic quantum conductance of a multiwalled carbon nanotube was observed at room temperature using the setup in TEM. It is concluded that *in situ* measurement by directly linking structure with property is a future direction of electron microscopy.

**Key words:** nanobelt, nanotube, *in situ* TEM

### INTRODUCTION

Nanowires, nanobelts, nanoribbons, nanorods, and so on are a new class of quasi-one-dimensional materials that have attracted much research interest in the last few years (Wang, 2003). These noncarbon-based materials have been demonstrated to exhibit superior electrical (Bjork et al., 2002; Gudixsen et al., 2002), optical (Huang et al., 2001; Duan et al., 2003), mechanical (Bai et al., 2003a), and thermal properties (L. Shi, Q. Hao, C. Yu, D. Kim, N. Mingo, X.Y. Kong, & Z.L. Wang, submitted), and can be used as fundamental building blocks for nanoscale science and technology, ranging from chemical and biological sensors (Cui et al., 2001; Comini et al., 2002) and field effect transistors (Arnold et al., 2003) to logic circuits (Duan et al., 2001). Nanowire- and nanobelt-based quasi-one-dimensional materials are the new focal point of research.

Transparent conducting metal oxides are fundamental to the development of smart and functional materials, which are candidates for optics, optoelectronics, and chemical, biochemical, and environmental sensors as well as transducers (Ginley & Bright, 2000). The oxides have two unique structural features, switchable and/or mixed cation valences and adjustable oxygen deficiency, that are the bases for creating many novel materials with unique electronic, optical, and chemical properties (Wang & Kang, 1998). The

oxides are usually made into nanoparticles or thin films to enhance their surface sensitivity. We have recently synthesized a nanobelt structure of a group of oxides and demonstrated their morphology and structural control (Pan et al., 2001a). In this article, we first review our current progress in the synthesis of oxide nanobelt structure. Then the mechanical properties of the nanobelts will be measured by an *in situ* transmission electron microscopy (TEM) technique, showing the dual-mode electromechanical resonance. Finally, we demonstrate the principle of applying *in situ* TEM for measuring the work function at the tip of a carbon nanotube and the electric transport through a carbon nanotube. It is pointed out that correlating the structure with property from the same nanostructure is a future direction of electron microscopy.

### NANOBELTS—A STRUCTURALLY CONTROLLED NANOMATERIALS SYSTEM

Recently, our group has reported a new class of distinctly different semiconducting oxide nanostructures that have a rectangular cross section, in correspondence to a beltlike morphology (so-called nanobelts; Pan et al., 2001a). The oxides with the nanobelt morphology include ZnO, SnO<sub>2</sub>, In<sub>2</sub>O<sub>3</sub>, CdO, Ga<sub>2</sub>O<sub>3</sub> (Pan et al., 2001a), PbO<sub>2</sub> (Pan et al., 2001b), and ZnS (Ma et al., 2003) covering cations with different valence states and materials with different crystallographic structures. Except for PbO<sub>2</sub> and ZnS, the other five oxides have long been regarded as transparent conduct-

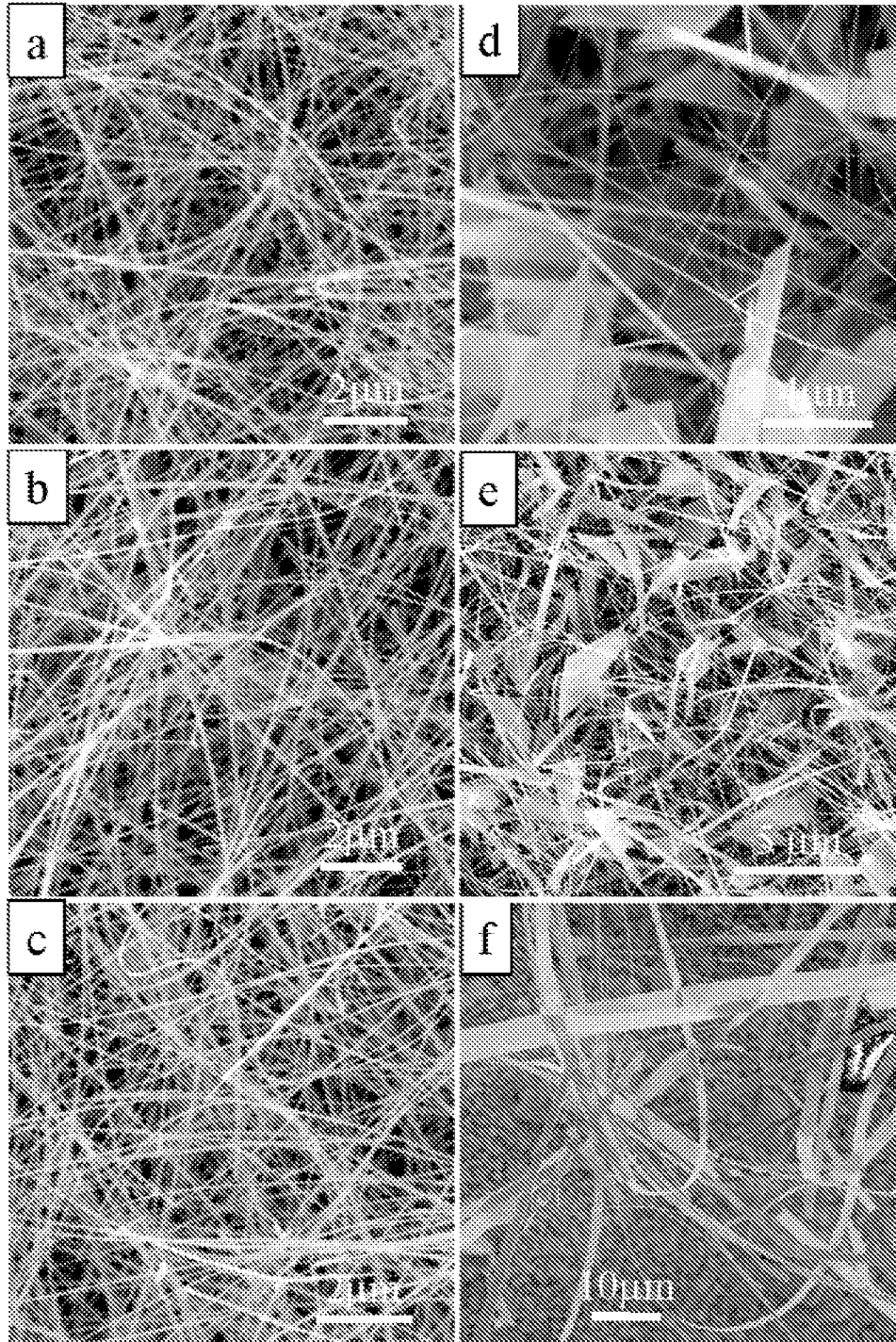


**Figure 1.** Typical SEM images taken from samples of (a) ZnO, (b) SnO<sub>2</sub>, (c) In<sub>2</sub>O<sub>3</sub>, (d) CdO, (e) Ga<sub>2</sub>O<sub>3</sub>, and (f) ZnS.

ing oxide (TCO) materials and have found wide applications in architectural glass, sensors, flat panel display, and so forth due to their distinctive optical, electrical, and thermal properties. The synthesis was based on a solid–vapor process by vaporizing solid powder at a high temperature zone; then a deposition at a lower temperature region results in

the formation of the nanobelt structure. Figure 1 shows a group of SEM images recorded from a few oxide nanobelt and nanosheet structures.

Transmission electron microscopy and electron diffraction are the two most powerful approaches for defining the structures of the nanobelts. Figure 2 shows some typical

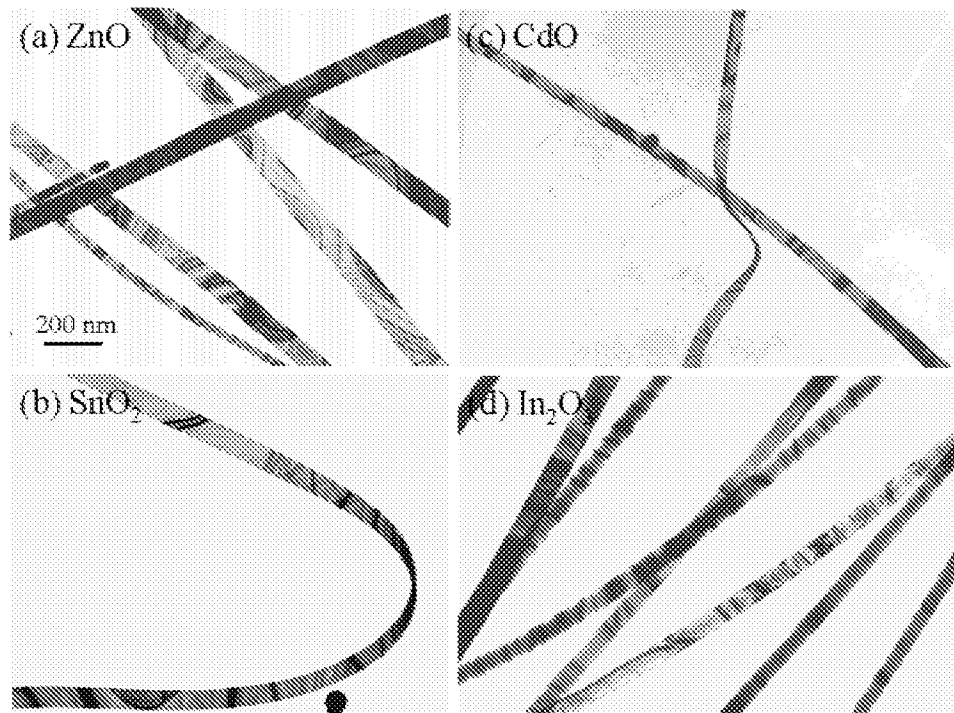


**Figure 2.** Typical TEM images of nanobelts made of (a) ZnO, (b) SnO<sub>2</sub>, (c) CdO, and (d) In<sub>2</sub>O<sub>3</sub>.

low-magnification TEM images of the oxide nanobelts, where the ribbon shape is apparent. We have carried out a systematic structure analysis of the as-synthesized nanobelt structure. Take ZnO as an example: The growth direction can be either  $[0001]$  or  $[01\bar{1}0]$ , whereas the top and bottom surfaces are  $(2\bar{1}\bar{1}0)$ . The nanobelts are single crystalline without the presence of line defects. A summary on the oxide systems that we have successfully synthesized into nanobelts and their corresponding growth directions and side and top surfaces are given in Table 1. The surfaces of the nanobelts are clean, atomically sharp, and without any sheathed amorphous phase. The as-synthesized nanobelts may belong to different crystallographic families, but they have a common shape that is the ribbon geometry. This is a unique and distinct structure character of the nanobelts.

## NANOBELT AS NANORESONATORS

The geometrical shape and the large mechanical flexibility of the nanobelts suggest that they can be ideal nanoresonators for nano/micromechanical systems. Due to the small size of the nanobelts, an alternative approach has to be used to examine their resonance behavior. We have previously observed the resonance behavior and measured the bending modulus of carbon nanotubes by an *in situ* transmission electron microscopy (TEM) technique (Poncharal et al., 1999; Wang et al., 2000b). Based on the electric-

**Table 1.** Semiconductive Oxide Nanobelts and Their Growth Directions and Surface Planes

Nanobelts	Crystal structure	Growth direction/plane	Top surface	Side surfaces
ZnO	Wurtzite	$[0001]$	$\pm(2\bar{1}\bar{1}0)$	$\pm(01\bar{1}0)$
ZnO	Wurtzite	$[01\bar{1}0]^a$	$\pm(2\bar{1}\bar{1}0)$	$\pm(0001)$
Ga <sub>2</sub> O <sub>3</sub>	Monoclinic	$[001]$	$\pm(100)$	$\pm(010)$
Ga <sub>2</sub> O <sub>3</sub>	Monoclinic	$[010]$	$\pm(100)$	$\pm(10\bar{1})$
SnO <sub>2</sub>	Rutile	$[101]$	$\pm(10\bar{1})$	$\pm(010)$
In <sub>2</sub> O <sub>3</sub>	C-Rare earth	$[001]$	$\pm(100)$	$\pm(010)$
CdO	NaCl	$[001]$	$\pm(100)$	$\pm(010)$
PbO <sub>2</sub>	Rutile	$[010]$	$\pm(201)$	$\pm(10\bar{1})$
ZnS	Wurtzite	$[0001]$	$\pm(2\bar{1}\bar{1}0)$	$\pm(01\bar{1}0)$

<sup>a</sup>The nanobelts have a single stacking fault/twin parallel to the growth direction throughout the entire length.

field-induced resonant excitation, mechanical properties of carbon nanotubes (Poncharal et al., 1999; Gao et al., 2000) and silicon carbide-silica composite nanowires (Wang et al., 2000a) have been quantified.

To carry out the mechanical property measurements of a nanobelt, a specimen holder for a Hitachi HF-2000 TEM (200 kV) was built for applying a voltage across a nanobelt and its count electrode. Mechanical resonance can be induced if the applied frequency matches the natural

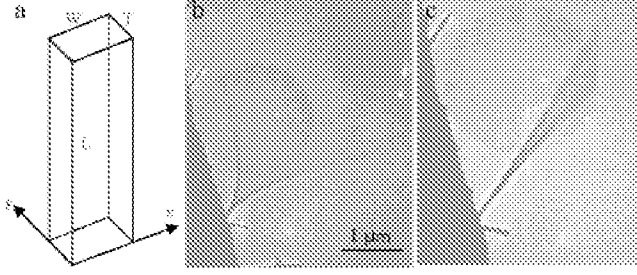


**Figure 3.** Measuring the bending modulus of a ZnO nanobelt by electric-field-induced mechanical resonance in TEM. **a:** Geometrical shape of a nanobelt; **b,c:** mechanical resonance of a nanobelt along the two orthogonal directions, respectively, closely perpendicular to the viewing direction ( $\nu_x = 1.25$  MHz), and nearly parallel to the viewing direction ( $\nu_y = 1.38$  MHz).

resonance frequency of the nanobelt. Due to the mirror symmetry of the nanobelt (Fig. 3a), there are two distinct fundamental resonance frequencies corresponding to the vibration in the thickness and width directions, respectively, which are given from the classical elasticity theory as (Meirovich, 1986)

$$\nu_x = \frac{\beta_1^2 T}{4\pi L^2} \sqrt{\frac{E_x}{3\rho}}, \quad (1)$$

$$\nu_y = \frac{\beta_2^2 W}{4\pi L^2} \sqrt{\frac{E_y}{3\rho}}, \quad (2)$$

where  $\beta_i$  is a constant for the  $i$ th harmonic:  $\beta_1 = 1.875$  and  $\beta_2 = 4.694$ ;  $E_x$  and  $E_y$  are the bending modulus if the vibration is along the  $x$ -axis (thickness direction) and the  $y$  direction (width direction), respectively; and  $\rho$  is the density,  $L$  is the length,  $W$  is the width, and  $T$  is the thickness of the nanobelt. The two modes are decoupled, and they can be observed separately.

Changing the frequency of the applied voltage, we found two fundamental frequencies in two orthogonal directions transverse to the nanobelt. Figure 3b,c shows the harmonic resonance with the vibration planes nearly perpendicular and parallel to the viewing direction, respectively (Bai et al., 2003a). For calculating the bending modulus, it is critical to accurately measure the fundamental resonance frequency ( $\nu_1$ ) and the dimensional sizes ( $L$  and  $T$  or  $W$ ) of the investigated ZnO nanobelt. The specimen holder is rotated about its axis so that the nanobelt can be aligned perpendicular to the electron beam, so the real length ( $L$ ) of the nanobelt can be measured. The projection direction along the beam is determined by electron diffraction, so that the true thickness and width can be determined because the normal direction of the nanobelt is  $[2\bar{1}\bar{1}0]$ . Based on the experimental data, the bending moduli of the ZnO nanobelts can be calculated using either equation (1) or (2).

**Table 2.** The Bending Modulus of Individual ZnO Nanobelts<sup>a</sup>

Nanobelt	Length $L$ ( $\mu\text{m}$ ; $\pm 0.05$ )	Thickness $T$ (nm; $\pm 1$ )	Frequency $\nu_{x1}$ (kHz)	Bending modulus $E$ (GPa)
1	8.25	33	232	$50.1 \pm 1.8$
2	4.73	19	396	$45.5 \pm 2.9$
3	4.07	20	662	$64.6 \pm 2.3$
4	8.90	39	210	$39.9 \pm 1.2$

<sup>a</sup>Our experiments found there is no significant difference between  $E_x$  and  $E_y$  for the nanobelt grown along  $[0001]$ .

The experimental results are summarized in Table 2 (Bai et al., 2003a). The bending modulus of the ZnO nanobelts was  $\sim 52$  GPa. This experiment unambiguously shows that the nanobelt can be an ideal nanoresonator exhibiting two orthogonal resonance modes, which could be used as probes for scanning probe microscopy (SPM) operated in tapping and scanning modes.

## NANOBELTS AS NANOCANTILEVER

The cantilever-based SPM technique is one of the most powerful approaches in imaging, manipulating, and measuring nanoscale properties and phenomena. The conventional cantilever used for SPM is based on silicon,  $\text{Si}_3\text{N}_4$  or  $\text{SiC}$ , which is fabricated by the e-beam or optical lithography technique and has typical dimension of thickness  $\sim 100$  nm, width  $\sim 5$   $\mu\text{m}$ , and length  $\sim 50$   $\mu\text{m}$ . Utilization of a nanowire- and nanotube-based cantilever can have several advantages for SPM. Carbon nanotubes have been grown on the tip of a conventional cantilever and are used for imaging surfaces with a large degree of abrupt variation in surface morphology (Dai et al., 1996). We demonstrate here that nanobelts can be nanocantilevers (Hughes & Wang, 2003).

The cantilevers under consideration are simple in design. Using a Dimension 3000 SPM in tapping mode, we have successfully lifted ZnO nanobelts from a silicon substrate. Combining the aforementioned techniques with micromanipulation has led to the alignment of individual ZnO nanobelts onto silicon chips (Fig. 4). The aligned ZnO cantilevers were manipulated to have a range of lengths. This exemplifies our ability to tune the resonance frequency of each cantilever and thus modify cantilevers for different applications such as tapping and contact mode AFM. The nanobelt-based nanocantilever is  $\sim 50$ – $100$  times smaller than the conventional cantilever. The reduced dimensions of the nanobelt cantilevers could offer a significant improvement in sensitivity.

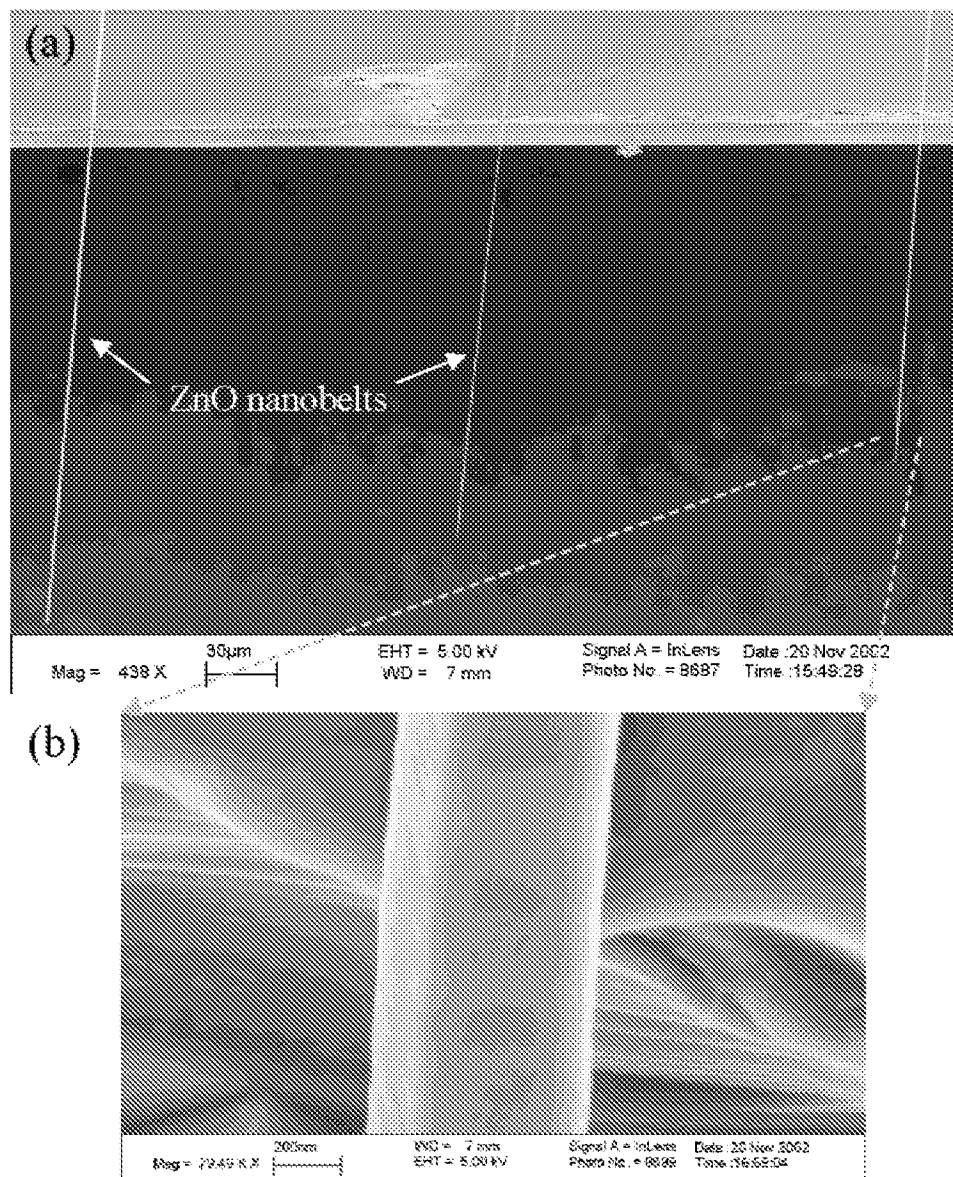


**Figure 4.** **a:** Site-specific placement and alignment of ZnO nanobelts onto a silicon chip, forming nanocantilever arrays. **b:** An enlarged SEM image of the third nanocantilever showing its shape; the width of the cantilever was measured to be 525 nm.

We have also fabricated field-effect transistors (FETs) based on single  $\text{SnO}_2$  and ZnO nanobelts of thicknesses between 10 nm and 30 nm (Arnold et al., 2003). Switching ratios as large as six orders of magnitude and conductivities as high as  $15 (\Omega\text{-cm})^{-1}$  are observed. Annealing  $\text{SnO}_2$  nanobelt FETs in an oxygen-deficient atmosphere produces a negative shift in gate threshold voltage, indicating doping by the generation of surface oxygen vacancies. This treatment provides an effective way of tuning the electrical performance of the nanobelt devices. The ability of  $\text{SnO}_2$  FETs to act as gas sensors is also demonstrated. ZnO nanobelt FETs are sensitive to ultraviolet light. Both photogener-

ation of electron-hole pairs and doping by UV-induced surface desorption contribute to the conductivity.

Gas sensors have also been fabricated using the single crystalline  $\text{SnO}_2$  nanobelts (Comini et al., 2002). Electrical characterization showed that the contacts were ohmic, and the nanobelts were sensitive to environmental polluting species like CO and  $\text{NO}_2$  as well as ethanol for breath analyzers and food control applications. The sensor response, defined as the relative variation in conductance due to the introduction of the gas, is  $\Delta G/G = 4160\%$  for 250 ppm of ethanol and  $\Delta G/G = -1550\%$  for 0.5 ppm nitrogen dioxide at  $400^\circ\text{C}$  and 30% RH. The results demon-

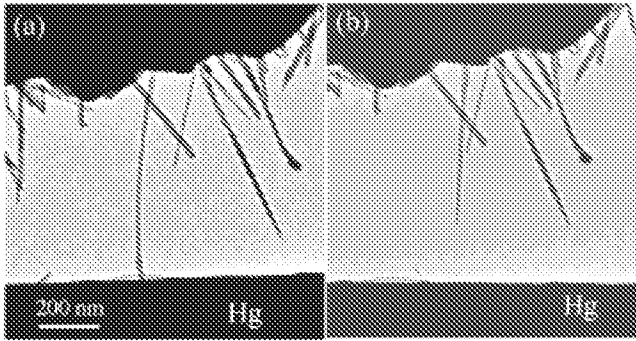


**Figure 5.** *In situ* observation of electric transport through a single carbon nanotube. **a:** Applied voltage  $V = 0.1$  V, current  $I = 7.3 \mu\text{A}$ , the resistance of the carbon  $R = 12.7 \text{ k}\Omega$ , which corresponds to a conductance  $G = (12.7 \text{ k}\Omega)^{-1} = 1.02G_0$ . **b:** After applying a 4-V voltage, the nanotube was broken and the break occurred at the contact of the nanotube and the Hg. **c:** The conductance of this carbon nanotube contaminated with graphitic particles is  $0.25G_0$ .

strate the potential for fabricating nanosize sensors using the integrity of a single nanobelt with sensitivity at the level of a few parts per billion.

## ELECTRIC TRANSPORT THROUGH A CARBON NANOTUBE

Measurement of electric transport through a single carbon nanotube can also be carried out in TEM (Wang et al., 2000c; Poncharal et al., 2002). Using the same specimen holder as used for mechanical property measurements, by changing the count electrode into a soft contacting metal, such as a tiny mercury droplet, a carbon nanotube can be directly put in contact with the electrode; thus, its transport property can be measured (Fig. 5a). The advantage offered by such a setup is that the nanotube can be directly imaged under an electron beam, while its electrical property is characterized. If the applied voltage is a fraction of a volt, the conductance of the nanotube is measured to be close to  $(12.7 \text{ k}\Omega)^{-1}$ , which is very close to the single channel conductance  $G_0 = 2e^2/h = (12.9 \text{ k}\Omega)^{-1}$  predicted by quantum mechanics. For a carbon nanotube without defects, the link between the graphitic sheets is weak, and there is little tunneling effect between the layers if the applied voltage is small. The current is effectively carried by the outermost layer, although the nanotube is multiwalled (Frank et al., 1998).

If the applied voltage is increased to 4 V, the nanotube burned out at the contacting point with the Hg electrode (Fig. 5b). This is due to the contact resistance between the nanotube and the mercury. At such a high voltage, tunneling between graphitic layers is strongly enhanced; thus, the

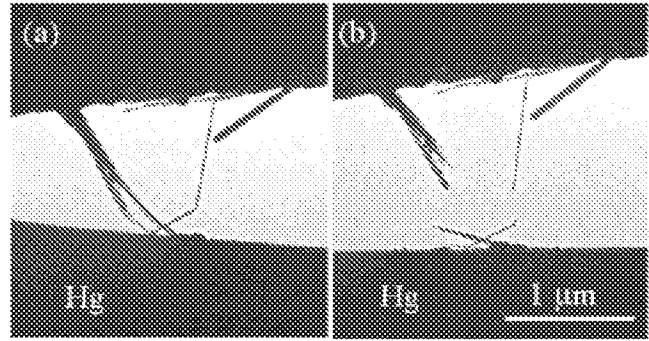


**Figure 6.** Examples of nanotube failure modes. Multiwalled carbon nanotube before (a) and after (b) passing a large current, showing the break points at the defect sites.

entire thickness of the wall would be effective for conducting current. The increased size of the conducting cross section leads to the disappearance of the quantum conductance effect.

We have previously shown that a defect-free nanotube can be a ballistic conductor without heat dissipation (Frank et al., 1998). However, at the junction of two nanotubes, defects must be introduced, such as the case shown in Figure 6a; thus, heat dissipation at the defects is possible. After applying a higher voltage, the burning point between the two nanotubes is just the junction point, as shown in Figure 6b. TEM provides powerful evidence for this transport phenomenon.

## WORK FUNCTION AT THE TIP OF A CARBON NANOTUBE

An important physical quantity in electron field emission is the surface work function, which is well documented for elemental materials. For the emitters such as carbon nanotubes (NTs), most of the electrons are emitted from the tips of the carbon NTs, and it is the local work function that matters to the properties of the NT field emission. The work function is measured from the  $\ln(J/E^2)$  versus  $1/E$  characteristics curve in the Fowler–Nordheim theory, where  $E$  is the macroscopic applied electric field that is an average over all of the aligned carbon NTs that are structurally diverse in diameters, lengths, and helical angles, and  $J$  is the emission current. We have developed an *in situ* TEM technique for the measurement of the work function at the tip of a single carbon nanotube (Gao et al., 2001).

Our measurement is based on the electric-field-induced mechanical resonance of carbon nanotubes, but with a slight modification. The principle for work function measurement is schematically shown in Figure 7a. We consider a simple case in which a carbon nanotube, partially soaked in a carbon fiber produced by arc discharge, is electrically

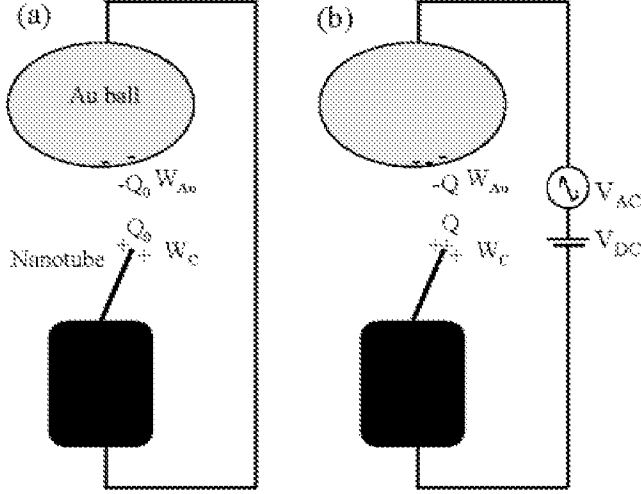


**Figure 7.** **a:** Schematic diagram showing the static charge at the tip of a carbon nanotube as a result of difference in work functions between the nanotube and the gold electrode. **b:** Schematic experimental approach for measuring the work function at the tip of a carbon nanotube.

connected to a gold ball. Because of the difference in the surface work functions between the NT and the counter Au electrode, a static charge  $Q_0$  exists at the tip of the NT to balance this potential difference even at zero applied voltage. The magnitude of  $Q_0$  is proportional to the difference between work functions of the Au electrode and the NT tip (NTT),  $Q_0 = \alpha(W_{Au} - W_{NTT})$ , where  $\alpha$  is related to the geometry and distance between the NT and the electrode.

The measurement relies on the mechanical resonance of the carbon NT induced by an externally applied oscillating voltage with tunable frequency. In this case, a constant voltage  $V_{DC}$  and an oscillating voltage  $V_{AC} \cos 2\pi ft$  are applied onto the NT, as shown in Figure 7b, where  $f$  is the frequency and  $V_{AC}$  is the amplitude. The total induced charge on the NT is

$$Q = Q_0 + \alpha e(V_{DC} + V_{AC} \cos 2\pi ft). \quad (3)$$

The force acting on the NT is proportional to the square of the total charge on the nanotube:

$$\begin{aligned} F &= \beta [Q_0 + \alpha e(V_{DC} + V_{AC} \cos 2\pi ft)]^2 \\ &= \alpha^2 \beta \{ [(W_{Au} - W_{NTT} + eV_{DC})^2 + e^2 V_{AC}^2 / 2] \\ &\quad + 2eV_{AC}(W_{Au} - W_{NTT} + eV_{DC}) \cos 2\pi ft \\ &\quad + e^2 V_{AC}^2 / 2 \cos 4\pi ft \} \end{aligned} \quad (4)$$

where  $\beta$  is a proportional constant. In equation (4), the first term is constant and it causes a static deflection of the

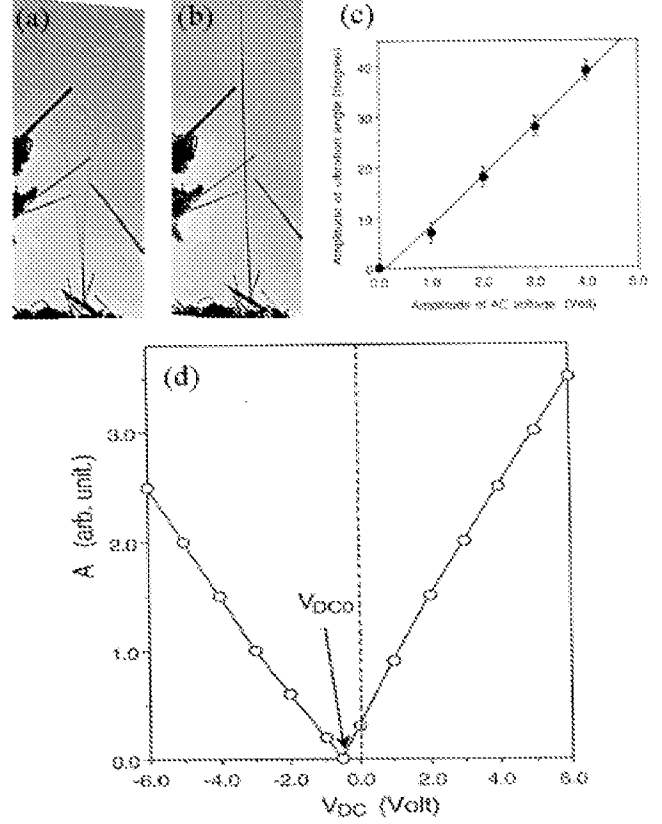


**Figure 8.** **a:** Mechanical resonance of a carbon nanotube induced by an oscillating electric field. **b:** Halting the resonance by meeting the condition of  $W_{Au} - W_{NTT} + eV_{DC0} = 0$ . **c:** A plot of vibration amplitude of a carbon nanotube as a function of the amplitude of the applied alternating voltage  $V_{AC}$ . **d:** A plot of vibration amplitude of a carbon nanotube as a function of the applied direct current voltage  $V_{DC}$ , while the applied frequency is 0.493 MHz and  $V_{AC} = 5$  V.

carbon NT; the second term is a linear term, and the resonance occurs if the applied frequency  $f$  approaches the intrinsic mechanical resonance frequency  $f_0$  of the carbon NT (Fig. 8a). The last term in equation (4) is the second harmonics. The most important result of equation (4) is that, for the linear term, the resonance amplitude  $A$  of the NT is proportional to  $V_{AC}(W_{Au} - W_{NTT} + eV_{DC})$ . By fixing the  $V_{DC}$  and measuring the vibration amplitude as a function of  $V_{AC}$ , a linear curve is received (Fig. 8c).

Experimentally, we first set  $V_{DC} = 0$  and tune the frequency  $f$  to find the mechanical resonance induced by the applied field. Second, under the resonance condition of keeping  $f = f_0$  and  $V_{AC}$  constant, slowly change the magnitude of  $V_{DC}$  from zero to a value that satisfies  $W_{Au} - W_{NTT} + eV_{DC0} = 0$  (Fig. 8b); the resonance amplitude  $A$  should be zero although the oscillating voltage is still in effect.  $V_{DC0}$  is the  $x$ -axis interception in the  $A \sim V_{DC}$  plot (Fig. 8d). Thus, the tip work function of the NT is  $W_{NTT} = W_{Au} + eV_{DC0}$ .

Several important factors must be carefully checked to ensure the accuracy of the measurements. The true fundamental resonance frequency must be examined to avoid higher-order harmonic effects. The resonance stability and frequency drift of the carbon nanotubes must be examined before and after each measurement to ensure that the reduction of vibration amplitude is solely the result of  $V_{DC}$ . The NT structure suffers no radiation damage at 100 kV, and the beam dosage shows no effect on the stability of the resonance frequency. The work function shows no sensitive dependence on the diameters of the NTs, at least in the range considered here. Seventy-five percent of the data indicate that the tip work function of carbon NTs is 0.3 to 0.5 eV lower than the work function of gold ( $W_{Au} = 5.1$  eV), whereas 25% of the data show that the tip work function is  $\sim 0.5$  eV higher than that of gold. In comparison to the work function of carbon ( $W_C = 5.0$  eV), the work function at the tip of a conductive multiwalled carbon NT is 0.2–0.4 eV lower. This is a merit for electron field emission. The technique demonstrated here has also been applied to measure the work function at the tip of a ZnO nanobelt and at the surface of a nanoparticle (Bai et al., 2003b).

## SUMMARY

In this article, we have reviewed our recent work on synthesis, characterization, and application of quasi-one-dimensional nanostructures. Nanobelts of semiconducting oxides of zinc, tin, indium, cadmium, and gallium have been synthesized by simply evaporating the desired commercial metal oxide powders at high temperatures. The as-synthesized oxide nanobelts are pure, structurally uniform, single crystalline, and most of them free from defects and dislocations; they have a rectangular-like cross section. The beltlike morphology appears to be a unique and common structural characteristic for the family of semiconducting oxides with cations of different valence states and materials of distinct crystallographic structures.

Electromechanical resonance of a single ZnO nanobelt, induced by an alternative electric field, has been observed by *in situ* TEM. The bending modulus of the ZnO nanobelts was measured to be  $\sim 52$  GPa. Because of the rectangular cross section of the nanobelt, two fundamental resonance modes have been observed in corresponding to the two orthogonal transverse vibration directions, showing the versatile applications of nanobelts as nanoresonators and nanocantilevers.

A novel technique has been developed for measuring the work function at the tip of a carbon nanotube. Ballistic conductance has been observed *in situ*. *In situ* TEM has also been demonstrated as a powerful tool for property measurement at the nano scale, with the capability of directly correlating the structure of a nanotube with its physical properties, which is a future direction of electron microscopy.

## ACKNOWLEDGMENTS

Dedicated to Professor J.M. Cowley on the occasion of his 80th birthday.

The materials reviewed in this article were partially contributed by my group members: Zhengwei Pan, Will Hughes, Xuedong Bai, Chris Ma, Daniel Moore, and Ruiping Gao, to whom I am grateful. Thanks for the support from the NASA URETI program and Georgia Tech. Thanks to Dr. Jingyue Liu for providing the SPM system used for cantilever manipulation.

## REFERENCES

- ARNOLD, M.S., AVOURIS, P.H., PAN, Z.W. & WANG, Z.L. (2003). Field-effect transistors based on single semiconducting oxides nanobelts. *J Phys Chem B* **107**, 659–663.
- BAI, X.D., WANG, E.G., GAO, P.X. & WANG, Z.L. (2003a). Dual-mode electromechanical resonance of individual ZnO nanobelts. *Appl Phys Lett* **82**, 4806–4808.
- BAI, X.D., WANG, E.G., GAO, P.X. & WANG, Z.L. (2003b). Measuring the work function at a nanobelt tip and at a nanoparticle surface. *NanoLetters* (in press).
- BJORK, M.T., OHLSSON, B.J., SASS, T., PERSSON, A.I., THELANDER, C., MAGNUSSON, M.H., DEPERT, K., WALLENBERG, L.R. & SAMUELSON, L. (2002). One-dimensional heterostructures in semiconductor nanowhiskers. *Appl Phys Lett* **80**, 1058–1060.
- COMINI, E., FAGLIA, G., SBERVEGLIERI, G., PAN, Z.W. & WANG, Z.L. (2002). Stable and high-sensitive gas sensors based on semiconducting oxide nanobelts. *Appl Phys Lett* **81**, 1869–1871.
- CUI, Y., WEI, Q.Q., PARK, H.K. & LIEBER, C.M. (2001). Nanowire nanosensors for highly sensitive and selective detection of biological and chemical species. *Science* **293**, 1289–1292.
- DAI, H.J., HAFNER, J.H., RINZLER, A.G., COLBERT, D.T. & SMALLEY, R.E. (1996). Nanotubes as nanoprobe in scanning probe microscopy. *Nature* **384**, 147–150.
- DUAN, X.F., HUANG, Y., AGARWAL, R. & LIEBER, C.M. (2003). Single-nanowire electrically driven lasers. *Nature* **421**, 241–245.
- DUAN, X.F., HUANG, Y., CUI, Y., WANG, J. & LIEBER, C.M. (2001). Indium phosphide nanowires as building blocks for nanoscale electronic and optoelectronic devices. *Nature* **409**, 66–69.
- FRANK, S., PONCHARAL, P., WANG, Z.L. & DE HEER, Z.L. (1998). Carbon nanotube quantum resistors. *Science* **280**, 1744–1746.
- GAO, R.P., PAN, Z.W. & WANG, Z.L. (2001). Work function at the tips of multi-walled carbon nanotubes. *Appl Phys Lett* **78**, 1757–1759.
- GAO, R.P., WANG, Z.L., BAI, Z.G., DE HEER, Z.G., DAI, L.M. & GAO, M. (2000). Nanomechanics of aligned carbon nanotube arrays. *Phys Rev Lett* **85**, 622–655.
- GINLEY, D.S. & BRIGHT, C. (2000). Transparent conducting oxides. *MRS Bull*, August, 15–18.
- GUDIKSEN, M.S., LAUHON, L.J., WANG, J.F., SMITH, D.C. & LIEBER, C.M. (2002). Growth of nanowire superlattice structures for nanoscale photonics and electronics. *Nature* **415**, 617–620.
- HUANG, M.H., MAO, S., FEICK, H., YAN, H.Q., WU, Y.Y., KIND, H., WEBER, E., RUSSO, R. & YANG, P.D. (2001). Room-temperature ultraviolet nanowire nanolasers. *Science* **292**, 1897–1899.

- HUGHES, W. & WANG, Z.L. (2003). Nanobelt as nanocantilever. *Appl Phys Lett* **82**, 2886–2888.
- MA, C., MOORE, D., LI, J. & WANG, Z.L. (2003). Nanobelts, nanocombs and nano-windmills of wurtzite ZnS. *Adv Mater* **15**, 228–231.
- MAO, S.X., ZHAO, M.H. & WANG, Z.L. (2002). Probing nano-scale mechanical properties of individual semiconducting nanobelt. *Appl Phys Lett* **83**, 993–995.
- MEIROVICH, L. (1986). *Elements of Vibration Analysis*. 2nd ed. New York: McGraw-Hill.
- PAN, Z.W., DAI, Z.R. & WANG, Z.L. (2001a). Semiconducting oxide nanobelts, *Science* **291**, 1947–1949.
- PAN, Z.W., DAI, Z.R. & WANG, Z.L. (2001b). Lead oxide nanobelts and phase transformation induced by electron beam irradiation. *Appl Phys Lett* **80**, 309–311.
- PONCHARAL, P., BERGER, C., YI, Y., WANG, Z.L. & DE HEER, W.A. (2002). Room temperature ballistic conduction in carbon nanotubes. *J Phys Chem* **106**, 12104–12118.
- PONCHARAL, P., WANG, Z.L., UGARTE, D. & DE HEER, W.A. (1999). Electrostatic deflections and electromechanical resonances of carbon nanotubes. *Science* **283**, 1513–1516.
- WANG, Z.L. (Ed.). (2003). *Nanowires and Nanobelts*. New York: Kluwer Academic Publisher.
- WANG, Z.L., DAI, Z.R., BAI, Z.G., GAO, R.P. & GOLE, J.L. (2000a). Side-by-side silicon carbide-silica biaxial nanowires: Synthesis, structure and mechanical properties. *Appl Phys Lett* **77**, 3349–3351.
- WANG, Z.L. & KANG, Z.C. (1998). *Functional and Smart Materials—Structural Evolution and Structural Analysis*. New York: Plenum Press.
- WANG, Z.L., PONCHARAL, P. & DE HEER, W.A. (2000b). Nano-measurements of individual carbon nanotubes by in-situ TEM. *Pure Appl Chem* **72**, 209–219.
- WANG, Z.L., PONCHARAL, P. & DE HEER, W.A. (2000c). Nano-measurements in transmission electron microscopy. *Microsc Microanal* **6**, 224–230.